Experimental Validation of a Time-Accurate Finite Element Model for Coupled Multibody Dynamics and Liquid Sloshing

Tamer M. Wasfy
Advanced Science and Automation Corp.
Indianapolis, IN

James O'Kins; Scott Smith
U.S. Army Tank Automotive Research Development and
Engineering Center, Warren, MI

ABSTRACT

A study for validating a time-accurate explicit finite element code for modeling fully-coupled flexible multibody systems carrying liquid-filled tanks is presented. The multibody system includes rigid bodies, flexible bodies, joints, and actuators. Rigid bodies rotational equations of motion are written in a body-fixed frame with the total rigid body rotation matrix updated each time step using incremental rotations. Flexible bodies are modeled using total-Lagrangian spring, truss, beam and hexahedral solid elements. A penalty model is used to impose the joint/contact constraints. An asperity-based friction model is used to model joint/contact friction. The fluid governing equations of motion are the incompressible Arbitrary Lagrangian-Eulerian Navier-Stokes equations along with a large-eddy simulation (LES) turbulence model. The fluid's free-surface is modeled using an acceptor-donor volume-of-fluid based algorithm. Coupling between the fluid and solid is achieved by solving Newton's equations of motions at the fluid-solid interface nodes.

The validation study is conducted using a multibody system consisting of a rigid baffled tank mounted on suspension springs. The springs are connected to a rigid frame mounted on two linear hydraulic-actuators. Experiments with various input ramp and harmonic excitation from the actuators are performed and the results of the experiments are compared to the results obtained using the model. The system response is measured using linear-displacement transducers at the springs and two cameras showing side and front views of the tank. The results show that the model can predict with reasonably good accuracy the test system's dynamic response.

1. INTRODUCTION

Many practical applications involve a flexible multibody system carrying one or more liquid filled tanks. The multibody system can be a ground vehicle (truck, train, or car), ship, airplane (commercial jet, military jet, or helicopter), a space vehicle (rocket or reusable launch vehicle) or a space structure (space station or satellite). The tank can be a payload tank or a liquid fuel tank. In those applications, an accurate computational model for predicting the coupled solid-fluid system response can greatly reduce the cost and time required to reach an optimum system design that satisfies the various operating constraints. The model must accurately account for the following effects:

- Incompressible liquid flow in a moving/deforming container.
- Modeling of the liquid free-surface.
- Modeling of turbulence and viscous effects.
- Coupling between the solid and the fluid at the fluid-structure interface.
- Large rotation of the solid bodies.
- Deformation of the solid flexible bodies. Flexible bodies can be modeled as beam, shells or general solids. For example a shell model can be used for a flexible tank.
- Joints kinematic constraints including joint friction and clearances.
- Frictional contact. For example for ground vehicle applications the rolling frictional contact of tires need to be accurately modeled.
- Actuators and control laws.
- Motion control components including transmission components, clutches, and brakes for ground vehicle applications. All those components involve friction.

The fluid flow is governed by the incompressible Navier-Stokes equations. Finite volume [1-3], finite element [4-6] or particle [7] discretization techniques have been used to model the fluid flow. Many techniques for modeling fluid flow with a free-surface have been developed in the literature. They include:

(a) *Volume-of-fluid (VOF) method* [8, 9]. Each element has a VOF value between 0 (for empty elements) and 1 (for elements completely filled with fluid). The free surface is reconstructed for each element using piecewise-linear planar segments that are calculated

1. REPORT DATE **16 APR 2007**	2. REPORT TYPE **N/A**	3. DATES COVERED **-**

4. TITLE AND SUBTITLE **Experimental Validation of a Time-Accurate Finite Element Model for Coupled Multibody Dynamics and Liquid Sloshing**	5a. CONTRACT NUMBER
	5b. GRANT NUMBER
	5c. PROGRAM ELEMENT NUMBER
6. AUTHOR(S) **O'Kins, James; Smith, Scott; Wasfy, Tamer M**	5d. PROJECT NUMBER
	5e. TASK NUMBER
	5f. WORK UNIT NUMBER
7. PERFORMING ORGANIZATION NAME(S) AND ADDRESS(ES) **US Army RDECOM-TARDEC 6501 E 11 Mile Rd Warren, MI 48397-5000**	8. PERFORMING ORGANIZATION REPORT NUMBER **17039**
9. SPONSORING/MONITORING AGENCY NAME(S) AND ADDRESS(ES)	10. SPONSOR/MONITOR'S ACRONYM(S) **TACOM TARDEC**
	11. SPONSOR/MONITOR'S REPORT NUMBER(S) **17039**

12. DISTRIBUTION/AVAILABILITY STATEMENT **Approved for public release, distribution unlimited**

13. SUPPLEMENTARY NOTES **Presented at the 2007 SAE World Congress, The original document contains color images.**

14. ABSTRACT

15. SUBJECT TERMS

16. SECURITY CLASSIFICATION OF:			17. LIMITATION OF ABSTRACT **SAR**	18. NUMBER OF PAGES **16**	19a. NAME OF RESPONSIBLE PERSON
a. REPORT **unclassified**	b. ABSTRACT **unclassified**	c. THIS PAGE **unclassified**			

from the VOF value of the element along with the VOF values of neighboring elements (which are used to determine the normal to the planar surface). When VOF algorithms were first used the free surface was reconstructed using either vertical or horizontal surfaces [8, 3]. The VOF values of all the elements are updated each time step by calculating the mass flux between elements. The mass flux for free-surface elements is calculated by taking into account the smaller surface through which the fluid can move due to the presence of the free surface.

(b) *Level-set method*. This method uses a smooth scalar function defined at every node in the fluid domain which specifies the signed smallest Eucledian distance between the node and the interface [5]. The evolution of the scalar function is governed by a convection transport equation where the interface is moved with the fluid velocity.

(c) *Arbitrary Lagrangian-Eulrian (ALE) method*. Using this method, the fluid mesh deforms and moves along with the fluid's free-surface [4, 6, 10]. A disadvantage of this method is that it does not allow large surface deformation including surface break-up and merging unless the fluid domain is re-meshed [11, 12]. If re-meshing is used frequently, it can degrade the solution accuracy due to re-interpolation of the solution field onto the new mesh.

(d) *Lagrangian particle methods.* Lagrangian particles which represent small packets of fluid are used to model the fluid flow. A contact model between the fluid particles is used to model the fluid compressibility and viscous effects. This method naturally handles free-surfaces. The main disadvantage of those types of methods is the large number of particles and computing time needed to accurately predict the fluid motion. A special type of this class of methods which has been successfully applied to free-surface flows and fluid-structure interaction problems is the particle finite element method (PFEM) [7] in which the particles are used to generate a polyhedral finite element mesh every time step using an extended Delaunay tesselation. The solution of the incompressible Navier-Stokes equations is then carried using that mesh. The PFEM requires less fluid particles, however, the tessellation step is computationally intensive. Particle methods can easily handle surface break-up and merging, floating bodies, and fluid-solid impenetrability boundary condition.

Techniques to handle fluid flow in a moving/deforming container include:

1. *Fixed Cartesian fluid mesh with cut-cell boundary condition*. The fluid domain is a Cartesian mesh. The container moves inside this mesh. A cut-cell technique is used to find where the boundary of the container intersects with the fluid cells. The cut-cell surfaces are then used to impose wall impenetrability and adhesion boundary conditions [1, 2]. The fixed Cartesian mesh has the advantage that

mesh generation is straightforward. In addition, it allows modeling floating objects and tank baffles with no additional effort. However, the main disadvantage of the technique is that the fluid-solid impenetrability and no-slip boundary conditions are satisfied only in a time average sense. Also, the method has stability and accuracy problems when the cut-cell elements at the solid-fluid interface become small.

2. *Moving ALE mesh*. The fluid is modeled using a fluid mesh that moves and deforms with the tank.

3. Fixed-fluid mesh with the Navier-Stokes equations written in a reference frame fixed to the tank [4, 13]. Since the tank frame is a non-inertial frame (accelerating frame), writing the equations of motion with respect to that frame results in a complex inertia operator which involves centrifugal and coriolis acceleration terms. Also, this method cannot - by itself - deal with a deforming container.

4. Particle methods. Normal contact constraint between the particles and the tank wall is used to model the wall impenetrability constraint. Tangential friction between the particles and the tank wall is used to model wall adhesion and viscous effects.

In order to model fluid flow with a free-surface in a moving deforming container, the above methods must be combined. Table 1 shows the references where the various combinations of the above techniques were used.

Table 1 References for the various combinations of techniques for modeling a free-surface flow in moving deforming container.

Free surface model	Moving / deforming tank model	Fixed grid	ALE	NS written in tank frame	Particles
VOF		1, 2	Present paper	13	
Level-set			5		
ALE			4, 6, 10, 11, 12	4	
Particles					6

In the present paper, an ALE mesh is used for modeling the moving/deforming container along with a VOF free-surface model. This method does not suffer from the cut-cell solid-fluid interface boundary-condition problem like the fixed grids with cut-cell boundary condition methods. It also allows modeling surface break-up and merging without the need for re-meshing.

A review of multibody dynamics modeling techniques including deformation reference frames, treatment of large rotations, discretization techniques, finite elements, constraint and contact modeling, and solution techniques is presented in [14]. In the present paper, a flexible multibody dynamics code with the following characteristics is used:

- An explicit time-integration solver accurate for long simulation times [15].

- Total Lagrangian, total displacement equations of motion formulation with the degrees of freedom referred to a global inertial reference frame [15-18].

- A library of truss, beam, and solid nonlinear finite elements with Cartesian coordinate degrees of freedom allowing arbitrarily large element rotations. Those include:

    o Torsional-spring type 3-node beam elements [15, 16].

    o Natural-modes eight-node brick elements [17, 18]. Those elements can also be used to model shells and beams. One element through the thickness is sufficient to accurately model the membrane, shear, and bending characteristics. They do not exhibit locking or spurious modes (widely used techniques to alleviate locking such as hourglass control lead to elements that do not maintain solution accuracy over very long solution times). They are computationally efficient. Assumed strain elements of comparable accuracy are more computationally expensive. Any material law can be used with those elements including: linear elastic, hyper-elastic, and non-linear laws.

- Penalty formulation for modeling joints (spherical, revolute, cylindrical and prismatic) [19].

- Rigid body rotational equations of motion are written in a body (material) frame, with the resulting incremental rotations added to the total body rotation matrix [19].

- Normal contact modeled using a penalty formulation [20, 21].

- Frictional contact modeled using an accurate and efficient asperity-based friction model [22].

- Special elements for modeling wheels/pulleys [20], sprockets [23], and clutches [24].

- General tire model [21]. The model includes the details of the tire construction. The tire rubber is modeled using brick elements. The bead, tread and ply are modeled using beam elements along the tire circumference and meridian directions with appropriate stiffness and damping properties. Normal contact between the tire and the wheel and between the tire and the pavement is modeled using the penalty technique. Friction is modeled using an asperity-based approximate Coulomb friction model. The tire inflation pressure is modeled by applying a force normal to the inner surface elements of the tire with the out-of-equilibrium force and moment applied to the wheel to guarantee self-equilibrium of the tire and wheel under the pressure load [21].

- General contact search algorithm that finds the contact penetration between finite elements and other elements as well as general triangle and quadrilateral surfaces.

Two-way coupling between the multibody system (vehicle) motion and the fluid is achieved by satisfying the following conditions at the solid-fluid interface:

- The fluid velocity normal to the solid's surface must be equal to the normal solid velocity.

- The fluid velocity tangent to the solid surface can range from being equal to the tangential velocity of the solid surface (no slip condition) to being free.

- No additional energy or momentum to the system should be introduced at the interface.

The above boundary conditions are satisfied by using Newton's equations of motion to find a common normal acceleration for the fluid and the solid at the interface. The tangential fluid and solid accelerations can range from being the same (no-slip condition) to being completely decoupled.

In the present paper, a single computational code which uses a time-accurate explicit solution procedure is used to solve both the solid and fluid equations of motion. Many commercial software and studies on modeling liquid sloshing coupled with solid body motion use two codes which pass the interface forces and motion back and forth and iterate on the two codes until equilibrium is achieved [e.g. 3, 13]. This approach adds additional computational burden and, in general, does not achieve the same accuracy as the single integrated code solution due to the difficulty in achieving an equilibrium solution between two disjoint codes.

The finite element code is validated by comparing its response prediction with the results from a multibody system consisting of a rigid baffled tank mounted on suspension springs. The springs are connected to a rigid frame which is mounted on two linear hydraulic-actuators. Using the actuators, the frame can be moved in pitch, roll and combination pitch/roll. A test matrix with different combinations of frame motions, tank fill levels (empty or half-full), and excitation types (ramp or harmonic) is carried out. The system response is measured using linear-displacement transducers at the suspension springs and two cameras showing side and front views of the tank along with the free-surface motion. Comparisons of the experimental results with the results generated using the finite element code are presented.

The rest of this paper is organized as follows. In Sections 2 and 3 the equations of motion for the solid and fluid are presented. In Section 4 the fluid-structure coupling model is presented. In Section 5 the VOF free-surface model is presented. In Section 6 the overall explicit solution procedure is outlined. In Section 7 the validation study along with the experimental setup are presented. Finally, in Section 8 some concluding remarks are offered.

2. SOLID EQUATIONS OF MOTION

In the subsequent equations the following conventions will be used:

- The indicial notation is used.
- The Einstein summation convention is used for repeated subscript indices unless otherwise noted.
- Upper case subscript indices denote node numbers.
- Lower case subscript indices denote vector component number.
- The superscript denotes time.
- A superposed dot denotes a time derivative.

The translational equations of motion are written with respect to the global inertial reference frame and are obtained by assembling the element equations. The finite elements used here use only translational DOFs with no rotational DOFs. This is advantageous in terms of computational efficiency, accuracy, and robustness [14]. Those equation also include the rigid-body (such as the wheel) translational DOFs. The equations can be written as:

$$M_K \ddot{x}_{Ki}^t = F_{s\,Ki}^t + F_{a\,Ki}^t \qquad (1)$$

where t is the running time, K is the global node number (no summation over K; K=1→N where N is the total number of nodes), i is the coordinate number (i=1,2,3), a superposed dot indicates a time derivative, M_K is the lumped mass of node K, x is the vector of nodal Cartesian coordinates with respect to the global inertial reference frame, and $\ddot{x}$ is the vector of nodal accelerations with respect to the global inertial reference frame, F_s is the vector of internal structural forces, and F_a is the vector of externally applied forces, which include surface forces and body forces.

For each rigid body, a body-fixed material frame is defined. The rigid body is represented by one node located at the body's center of mass, which is also the origin of this frame. The mass of the body is concentrated at the node and the inertia of the body given by the inertia tensor I_{ij} is defined with respect to the body frame. The orientation of the body-frame is given by $R_K^{t_o}$ which is the rotation matrix relative to the global inertial frame at time t_0. The rotational equations of motions are written for each rigid body with respect to its body-fixed material frames as:

$$I_{Kij} \ddot{\theta}_{Kj}^t = T_{s\,Ki}^t + T_{a\,Ki}^t - \left(\dot{\theta}_{Ki}^t \times (I_{Kij} \dot{\theta}_{Kj}^t) \right)_{Ki} \qquad (2)$$

where I_K is the inertia tensor of rigid body K, $\ddot{\theta}_{Kj}$ and $\dot{\theta}_{Kj}$ are the angular acceleration and velocity vectors' components for rigid body K relative to it's material frame in direction j, T_{sKi} is the component of the vector of internal torque at node K in direction i, and T_{aKi} is the component of the vector of applied torque in direction i. The summation convention is used only for the lower case indices i and j.

The trapezoidal rule is used as the time integration formula for solving equations (1) for the global nodal positions x:

$$\dot{x}_{Kj}^t = \dot{x}_{Kj}^{t-\Delta t} + 0.5\,\Delta t\,(\ddot{x}_{Kj}^t + \ddot{x}_{Kj}^{t-\Delta t}) \qquad (3a)$$

$$x_{Kj}^t = x_{Kj}^{t-\Delta t} + 0.5\,\Delta t\,(\dot{x}_{Kj}^t + \dot{x}_{Kj}^{t-\Delta t}) \qquad (3b)$$

where Δt is the time step. The trapezoidal rule is also used as the time integration formula for the nodal rotation increments:

$$\dot{\theta}_{Kj}^t = \dot{\theta}_{Kj}^{t-\Delta t} + 0.5\,\Delta t\,(\ddot{\theta}_{Kj}^t + \ddot{\theta}_{Kj}^{t-\Delta t}) \qquad (4a)$$

$$\Delta \theta_{Kj}^t = 0.5\,\Delta t\,(\dot{\theta}_{Kj}^t + \dot{\theta}_{Kj}^{t-\Delta t}) \qquad (4b)$$

where $\Delta\theta_{Kj}$ are the incremental rotation angles around the three body axes for body K. The rotation matrix of body K (R_K) is then evaluated using:

$$R_K^t = R_K^{t-\Delta t}\, R(\Delta \theta_{Kj}^t) \qquad (5)$$

where $R(\Delta \theta_{Kj}^t)$ is the rotation matrix corresponding to the incremental rotation angles from Equation (4b).

The explicit solution procedure used for solving equations (1-5) along with constraint equations is presented in Section 6. The constraint equations are generally algebraic equations, which describe the position or velocity of some of the nodes. They include:

- Prescribed motion constraints:

$$f(\{x\}, t) = 0 \qquad (6)$$

- Joint constraints:

$$f(\{x\}) = 0 \qquad (7)$$

- Contact/impact constraints:

$$f(\{x\}) \ge 0 \qquad (8)$$

The penalty technique is used for imposing the constraints in which a normal reaction force is generated when a node penetrates into a contact body. The magnitude of the force is proportional to the penetration distance [20, 21]. An asperity-spring friction model is used to model joint and contact friction [22] in which friction is modeled using a piece-wise linear velocity-dependent approximate Coulomb friction element in parallel with a variable anchor point spring. The model approximates asperity friction where friction forces between two rough surfaces in contact arises due to the interaction of the surface asperities.

3. SEMI-DISCRETE FLUID EQUATIONS OF MOTION

The dynamic response of the fluid is described by the ALE version of the incompressible Navier-Stokes equations, namely, the equations of conservation of momentum and mass for a moving deforming control volume along with a large-eddy simulation (LES) transport equation. Those are:

$$\int_V \rho \frac{\partial u_i}{\partial t} dV = \int_V -u_i \frac{\partial \rho}{\partial t} dV + \int_V \frac{\partial [-\rho u_i \hat{u}_j - P\delta_{ij} + \tau_{ij}]}{\partial x_j} dV + \int_V \rho f_i dV \quad (9)$$

$$\int_V \frac{\partial \rho}{\partial t} dV + \int_V \frac{\partial (\rho \hat{u}_i)}{\partial x_i} dV = 0 \quad (10)$$

$$\rho = \rho_0 + r\,P \quad (11)$$

$$\hat{u}_i = u_i - v_i \quad (12)$$

$$\tau_{ij} = \lambda D_{kk} \delta_{ij} + 2(\mu + \mu_t) D_{ij} \quad (13a)$$

$$D_{ij} = 0.5(\partial \hat{u}_i / \partial x_j + \partial \hat{u}_j / \partial x_i) \quad (13b)$$

$$\int_V \frac{\partial (\rho K)}{\partial t} dV = -\int_V \frac{\partial (\rho \hat{u}_i K)}{\partial x_i} dV + \int_V \frac{\partial}{\partial x_i}\left[(\mu + \mu_t) \frac{\partial K}{\partial x_i}\right] dV + \quad (14)$$

$$\int_V \left(2\mu D_{ij} - \frac{2}{3} \rho K \, \partial_{ij}\right) \frac{\partial \hat{u}_i}{\partial x_j} dV - \int_V \rho \varepsilon \, dV$$

$$\varepsilon = 1.0 \, K^{3/2} \quad (15a)$$

$$\mu_t = 0.05 \sqrt{K} \quad (15b)$$

where V is the element volume, t is the running time, ρ is the density of the fluid, $\vec{u}$ is the fluid velocity vector relative to the global reference frame, $\hat{u}$ is the fluid velocity vector relative to the moving fluid mesh, $\vec{v}$ is the velocity of the fluid mesh, P is the relative pressure, $\vec{x}$ is the position vector, τ is the deviatoric stress tensor, D is the rate of deformation tensor, $\vec{f}$ is the body force vector, r is the artificial compressibility parameter, ρ_0 is the nominal fluid density, μ is the fluid viscosity, μ_t is an additional turbulence viscosity calculated using Equation 15b), K is the eddy kinetic energy, and ε is the sub-grid scale eddy kinetic energy dissipation term. Incompressible flow is modeled using the artificial compressibility technique [25]. A finite element formulation is used to derive the element's semi-discrete equations of motion from the governing equations (9-13). 8-node hexahedral elements are used with tri-linear equal-order velocity and pressure interpolation. A pressure averaging algorithm [26] is used to eliminate pressure checker-boarding (due to the use of an equal order interpolation for pressure and velocity). The element equations are assembled into the global semi-discrete equations of motion:

$$M_{f_N} \dot{u}_{Ni}^t = F_{f_{Ni}}^t \quad (16)$$

$$V_{f_N} \dot{P}_{Ni}^t = Q_{f_N}^t \quad (17)$$

$$M_{f_K} \dot{K}_N^t = S_{f_N}^t \quad (18)$$

where M_{f_N} is the lumped fluid mass of node N, $\dot{u}_{Ni}^t$ is component i of the fluid acceleration at node N, $F_{f_{Ni}}^t$ is component i of the fluid forces at node N, V_{f_N} is the lumped fluid volume at node N, $\dot{P}_N^t$ is the fluid pressure rate at node N, $Q_{f_N}^t$ is the fluid pressure flux at node N, $\dot{K}_N^t$ is the eddy kinetic energy rate at node N, and $S_{f_N}^t$ is the eddy kinetic energy flux at node N. Those equations are integrated using the trapezoidal rule along with an explicit solution procedure to yield the nodal fluid velocity and pressure:

$$u_{Kj}^t = u_{Kj}^{t-\Delta t} + 0.5\,\Delta t\,(\dot{u}_{Kj}^t + \dot{u}_{Kj}^{t-\Delta t}) \quad (19)$$

$$P_{Kj}^t = P_{Kj}^{t-\Delta t} + 0.5\,\Delta t\,(\dot{P}_{Kj}^t + \dot{P}_{Kj}^{t-\Delta t}) \quad (20)$$

$$K_{Kj}^t = K_{Kj}^{t-\Delta t} + 0.5\,\Delta t\,(\dot{K}_{Kj}^t + \dot{K}_{Kj}^{t-\Delta t}) \quad (21)$$

4. FLUID-STRUCTURE COUPLING MODEL

Newton's equations of motion are used to find a common normal acceleration for the fluid and the solid at the interface. This is done for each node at the fluid-structure boundary as follows:

$$(m_s + m_f)\vec{u}_n = \sum FluidForces + \sum StructureForces \quad (22a)$$

$$(m_s + m_f)\vec{v}_n = \sum FluidForces + \sum StructureForces \quad (22b)$$

where m_s is the solid mass of the node, m_f is the fluid mass of the node, $\vec{u}_n$ and $\vec{v}_n$ are respectively the fluid and solid accelerations of the node normal to the fluid-structure interface. The tangential fluid and solid accelerations $(\vec{u}_t, \vec{v}_t)$ are calculated using the following equations:

$$((1-s)m_s + m_f)\vec{u}_t = (1-s)\sum StructureForces + \sum FluidForces \quad (23a)$$

$$(m_s + (1-s)m_f)\vec{v}_t = \sum StructureForces + (1-s)\sum FluidForces \quad (23b)$$

where s is the slip factor. A no-slip condition corresponds to a slip factor of zero. The slip factor determines how much of the fluid and structure forces are mutually exchanged. Equations 22 and 23 are written for all fluid-solid interface nodes. The fluid mesh must move and deform with the tank. This is done by modeling the fluid mesh using very light and compliant (3 orders of magnitude less than the tank) solid brick elements (called "mock" mesh). The ALE formulation is used to account for the fluid mesh deformation/motion.

5. VOF FREE-SURFACE MODEL

For each fluid element a VOF value between 0 and 1 is defined, where 0 corresponds to empty elements and 1 corresponds to elements completely filled with fluid. The elements' VOF values are updated each time-step by moving fluid from a completely or partially filled "donor" element to an empty or partially filled neighboring "acceptor" element using the following model:

$$V_{eo} = V_e \; VOF_e \quad (24)$$

$$V_{na} = V_n \; (1 - VOF_n) \quad (25)$$

$$\Delta V = \begin{cases} \Delta t\, S\, A\, \vec{n}.\vec{u} & V_{eo} > \Delta V \;\; \text{and} \;\; V_{na} > V_{eo} \\ V_{eo} & V_{eo} < \Delta V \\ V_{na} & V_{na} < \Delta V \end{cases} \quad (26)$$

where V_e is the volume of the element; V_n is the volume of the neighboring element; V_{eo} is the volume of the element occupied by the fluid; V_{na} is the volume of the neighboring element available to receive fluid; ΔV is the volume flow through the boundary between the two elements in a time step; Δt is the solution time step; S is the surface area between the two elements; A is a value

between 0 and 1 indicating the free-surface aperture through which the fluid can move from the element to the neighboring element; $\vec{n}$ is a unit vector normal to *S*; and $\vec{u}$ is the fluid velocity vector at the surface *S*. If ΔV is less than 0 then the element is an acceptor element and the VOF values are not updated because they will be updated later when the neighbor element is set to be the donor element. If ΔV is greater than 0 then the VOF values are updated using the following equations:

$$\text{VOF}_e = \text{VOF}_e - \Delta V / V_e \qquad (27)$$
$$\text{VOF}_n = \text{VOF}_n + \Delta V / V_n \qquad (28)$$

The free-surface apertures *A* at the element interfaces are used to limit the fluid flow based on the location of the free surface inside the element. *A* is calculated as follows. If the VOF value of the element is 1 then there is no free-surface at the element, therefore *A*=1. For elements with a VOF value less than 1, the following steps are used to calculate *A*:

- Calculate the normal to the surface by looking at a stencil of neighboring elements around the element. This is done using the following equation:

$$n_{e_i} = \text{VOF}_{n_k} S_{n_k} n_{n_{ki}} \quad i=1, 2, 3 \qquad (29)$$

where n_{e_i} is the ith component of the normal to the free-surface at the element, VOF_{n_k} is the VOF value for neighboring element number k, S_{n_k} is the area of the intersection surface between the element and neighboring element k, and $n_{n_{ki}}$ is the component i of the normal to the surface between the element and neighboring element k. $\vec{n}_e$ is then normalized into a unit vector. Figure 1 shows a 2D 4-node quadrilateral and the free-surface along with the normal $\vec{n}_e$.

- Calculate the apertures A for each neighboring element by constructing a planar surface with normal $\vec{n}_e$ and with total volume equal to $\text{VOF}_e V_e$ (see Figure 1).
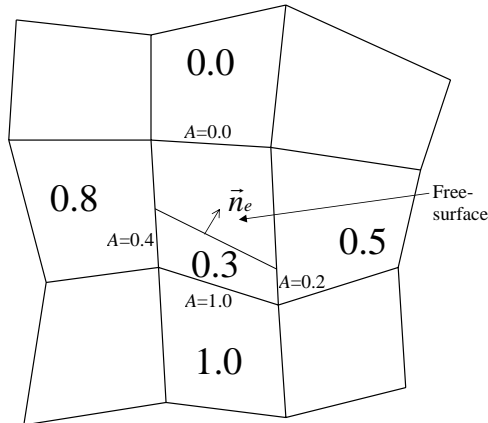
Figure 1 Stencil of neighboring elements used to determine the free-surface normal $\vec{n}_e$ and the liquid free-surface.

6. EXPLICIT SOLUTION PROCEDURE

The solution fields for modeling the solid, fluid and liquid free-surface are defined at the model nodes. These are:

- Solid translational positions.
- Solid translational velocities.
- Solid translational accelerations.
- Solid rotation matrices.
- Solid rotational (angular) velocities.
- Solid rotational (angular) accelerations.
- Fluid velocities.
- Fluid accelerations.
- Fluid pressure.
- Fluid pressure rate.
- Volume-of-fluid.
- Eddy kinetic energy
- Eddy kinetic energy rate.

The explicit time integration solution procedure for modeling the coupled response of the solid (multibody system), fluid, and liquid free-surface (using the VOF formulation) predicts the time evolution of the above response quantities. The procedure is implemented in the DIS [27] (Dynamic Interactions Simulator) commercial software code and is outlined below:

1) Prepare the run:
   a. Set the initial conditions for the solution fields identified above.
   b. Create a list of all the finite elements (including both solid and fluid elements).
   c. Create a list of elements that will run on each processor. This is done using an algorithm which tries to make the computational cost on each processor equal.
   d. Create a list of all the constraints (including both solid and fluid constraints).
   e. Calculate the solid masses for each finite element node by looping through the list of finite elements. Note that the solid masses are fixed in time.
   f. For each node create a list of corner and edge nodes that are connected to it using fluid volume elements.
   g. VOF preparations:
      i. Find a list of the volume fluid elements.
      ii. Create a list of fluid volume elements that will run on each processor. This is done using an algorithm which tries to make the computational cost on each processor equal.
      iii. For each element find all neighboring elements.
      iv. For each element find the element VOF using the nodal VOF.
      v. Re-interpolate the elements' VOF to nodal VOF.
   h. Loop over all the elements and find the minimum time step for the explicit solution procedure.
   i. Loop over all the elements and create a list of wall nodes. For each wall node find the list of fluid boundary elements.
2) Loop over the solution time and increment the time by Δt each step while doing the following:
   a. Set the nodal values at the last time step to be equal to the current nodal values for all solution fields.
   b. Do 2 iterations (a predictor iteration and a corrector iteration) of the following:

i. Initialize the nodal fluxes to zero. Those include: solid forces, solid moments, fluid forces, boundary fluid forces, and pressure fluxes. In addition, the lumped nodal fluid volume and fluid mass vectors are also initialized to zero.

ii. Calculate the nodal solid and fluid fluxes and the lumped fluid volume/mass vectors by looping through all the elements while calculating and assembling the element nodal fluxes and vectors. This is the most computational intensive step. This step is done in parallel by running each list of elements identified in step 1.c on one processor.

iii. Find the nodal values at the current time step using the semi-discrete equations of motion and the trapezoidal time integration rule (Equations 1-5 and 19-21).

iv. Execute the solid and fluid constraints. The constraints prescribe the nodal values.

v. Apply fluid-structure interface boundary conditions for all wall nodes found in Step 1.i (see Equations 22, 23). This is done by doing the following for each wall node:
   1. Find the normal to the surface at the wall node.
   2. Normalize the surface normal.
   3. Find the solid, fluid bulk and fluid boundary forces in the directions normal and tangent to the surface.
   4. Find the normal and tangential solid and fluid accelerations using the trapezoidal integration rule and the wall slip percentage.

vi. Set the pressure boundary conditions at the free surface.

vii. Update the VOF field:
   1. For each fluid element calculate the element volume. This step is done in parallel using the list of fluid elements for each processor found in Step 1.g.ii.
   2. For each fluid element find the apertures through which the fluid convects to each neighboring element. This step is done in parallel using the list of fluid elements for each processor found in Step 1.g.ii.
   3. For each fluid element use the apertures, the element volume, the element current VOF value, and the element nodal velocities to update the VOF value of all neighboring elements by finding the volume of fluid that left the element during that time step using Equations 24-28. This step is done in parallel using the list of fluid elements for each processor found in Step 1.g.ii. Note that this step depends on the order of the elements in the list of elements. However, since the updates of the VOF field between solution time steps are small, therefore this dependence is generally very small. In order to assure minimum dependence on the elements' order, at a time step the elements are updated from first to last, then at the next time step they are updated from last to first.

viii. Average the fluid pressure (This step eliminates the pressure checker-boarding effect and allows use of equal order interpolation for both pressure and velocity).

ix. Go to the beginning of step 2.

An advantage of explicit solution procedures is that they are "embarrassingly" parallel. The above procedure achieves near linear speed-up with the number of processors.

7. VALIDATION STUDY

A test fixture, located in TARDEC's Simulation Laboratory (TSL), was constructed to validate the computational code. The test fixture consists of an oval tank mounted on three suspension spring-dampers, which are in turn mounted on a rigid frame (Figure 2). Connecting rods along with spherical joints are used to constrain the horizontal (lateral and longitudinal) motion of the springs, such that they move nearly vertically. The frame is mounted on two linear hydraulic actuators which can be used to move the frame. When the actuators move the same way, then only the frame pitch angle is changed. When the actuators move in an opposing way, then the roll angle of the frame is changed. The test fixture is designed to simulate typical motions that a ground vehicle is subjected to. The pitch motion of the frame simulates both sides of the vehicle going over a bump. The roll motion simulates the vehicle turning or going over a bump only on one side of the vehicle.
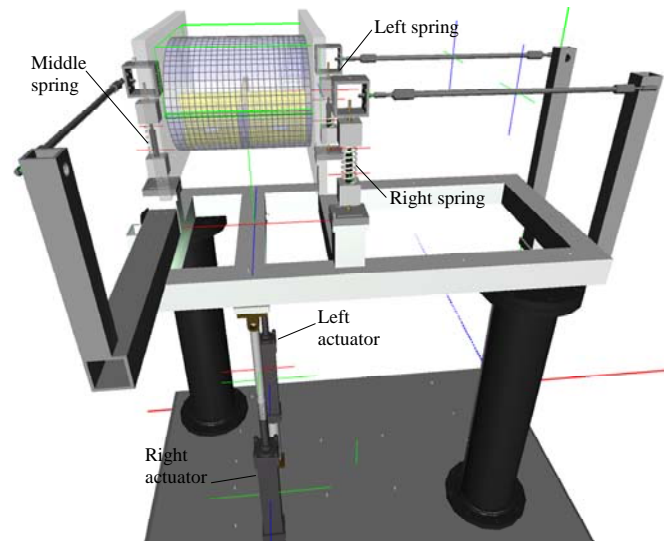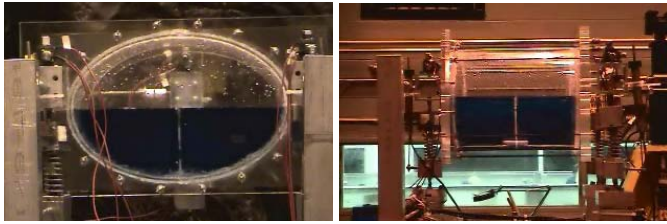

Figure 2 Test-fixture model.

The tank has longitudinal and cross-section baffles (Figure 3). The baffles have openings near the bottom of the tank to equalize the liquid level when the tank is less than half-full. The tank/baffles geometry and configuration are similar to typical army large-volume water/fuel tanks.
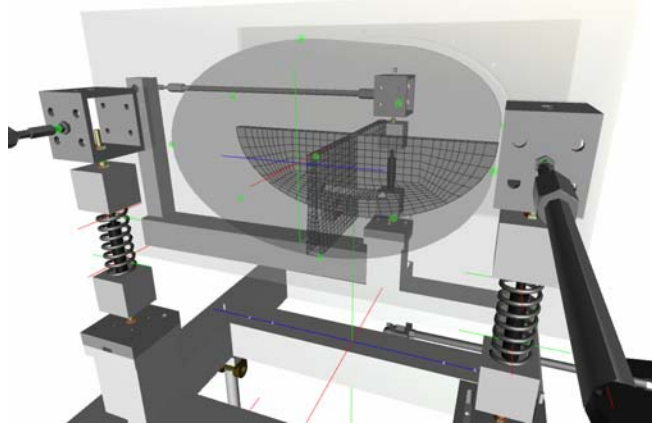
Figure 3 Tank longitudinal and cross-sectional baffles.

The linear input motion of the two actuators is measured using LVDTs. Also, the linear motion of the three suspension springs is measured using LVDTs. The signal of the LVDTs is sampled at 256 samples/sec. Two cameras are mounted on the ground to record the motion of the tank and sloshing of the liquid inside the tank. One camera shows the front view of the tank and the other camera shows the side view (Figure 4). The cameras are set to capture 30 frames/sec.

Figure 4 Front (left) and side (right) views of the tank using the two ground mounted cameras.

A DIS finite element model of the test fixture is constructed. The model consists of the following components:

- *An oval tank*. The tank dimensions are: 0.324 m length, width 0.428 m and height 0.276 m. The tank is modeled using shell elements.

- *Three linear suspension spring-dampers*. Each spring-damper consist of a linear compression spring in parallel with a linear strut. The struts were drained of fluid, but they still provide a small amount of viscous damping as well as Coulomb friction. The physical characteristics of the springs-struts are shown in Table 2. The struts are modeled using cylindrical joints.

- *The frame* is modeled as a rigid body. The springs are mounted to the frame using spherical joints.

- *Two linear actuators* connected to the frame.

- *A rigid grounded base*.

- *Connecting rods.* Provide horizontal (lateral and longitudinal) stability for the tank. The rods are connected to the tank and frame using spherical joints.

- *17 spherical joints*.

- 5 cylindrical joints located at the 3 suspension system springs and the two actuators.

Table 2 Physical characteristics of the test fixture spring-dampers.

	Left/Right spring	Middle spring
Stiffness	3200 N/m	8100 N/m
Damping	14 N sec/m	14 N sec/m
Friction force	6 N	6 N

The test fixture is simulated with an empty tank and with the tank half-full with water ($\rho = 1000$ Kg/m^3, $\mu = 0.001$ Kg/(m.sec). The water is modeled as incompressible using the artificial compressibility technique with an artificial sound speed factor of 0.1 (i.e. the artificial sound speed in the water is taken as 1483m/sec x 0.1 = 148.3 m/sec). Due to the use of large elements near the solid surface, full slip boundary condition at the wall is used ($s = 1$ in Equation 23). Thus, the viscous wall friction effects are assumed to be negligible. Gravity is modeled with the gravitational acceleration taken to be 9.8 m/sec^2 in the vertical direction.

**Table 3** Empty tank with baffles (Total of 12 experiments).

|	Pitch		Roll	
	Frequency (Hz)	Amplitude (mm)	Frequency (Hz)	Amplitude (mm)
Harmonic excitation	1.5	12	2	30
	2	12	3	20
	3	6	4	8
	Amplitude (mm)		Amplitude (mm)	
Ramp excitation	16		10	
	32		20	
	52		52	

Table 4 Half-full tank with baffles and half-full tank without baffles (Total of 24×2=48 experiments).

|	Pitch		Roll		Stir	
	Freq. (Hz)	Amplitude (mm)	Freq. (Hz)	Amplitude (mm)	Freq. (Hz)	Amplitude (mm)
Harmonic excitation	1.5	8	1.5	15	1.5	8
	1.5	12	1.5	30	1.5	16
	2	8	2	15	2	8
	2	12	2	30	2	16
	3	6	3	10	3	8
	3	8	3	20		
			4	8		
	Amplitude (mm)		Amplitude (mm)		Amplitude (mm)	
Ramp excitation	16		10		8/16	
	32		20		16/32 mm	

A test matrix consisting of 60 experiments was performed. Tables 3 and 4 show the input motion of the actuators for each experiment. The input motions types include pitch, roll and stir (combination pitch and roll) excitations. Recall that pitch motion means that the two actuators are moving in the same way (i.e. in phase) and roll excitation means that the two actuators are moving in an opposing way (i.e. 180° out of phase with each other when a harmonic excitation is used). For each motion type either a harmonic excitation or a ramp excitation was used. For the harmonic excitation the frequency and amplitude of the excitation is varied. For the ramp excitation just the amplitude of the excitation is varied.
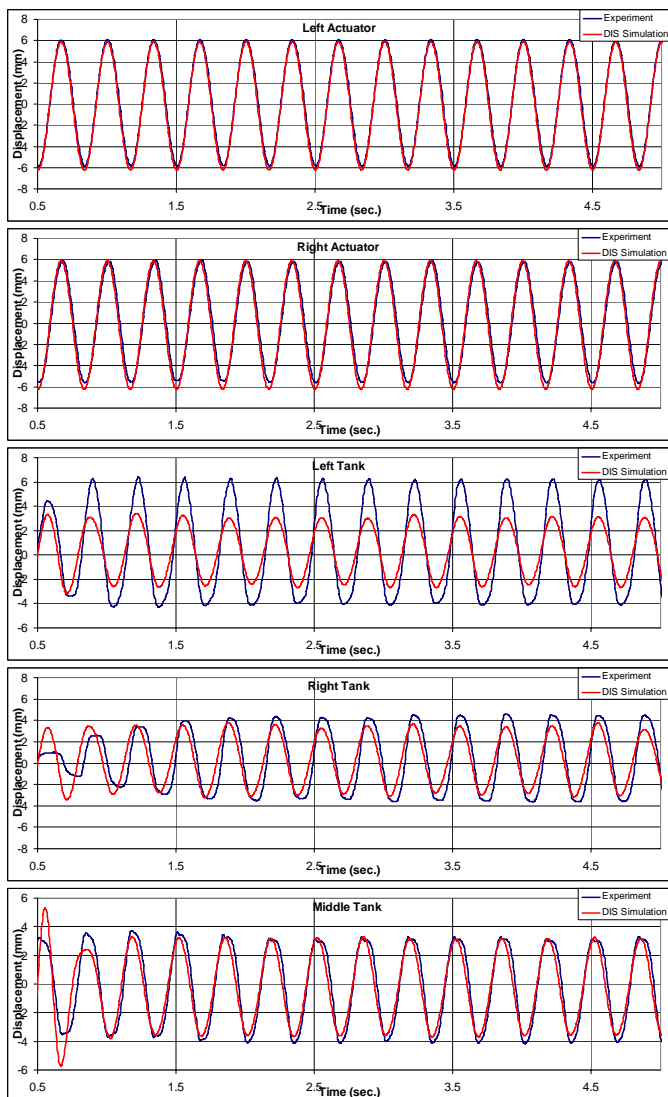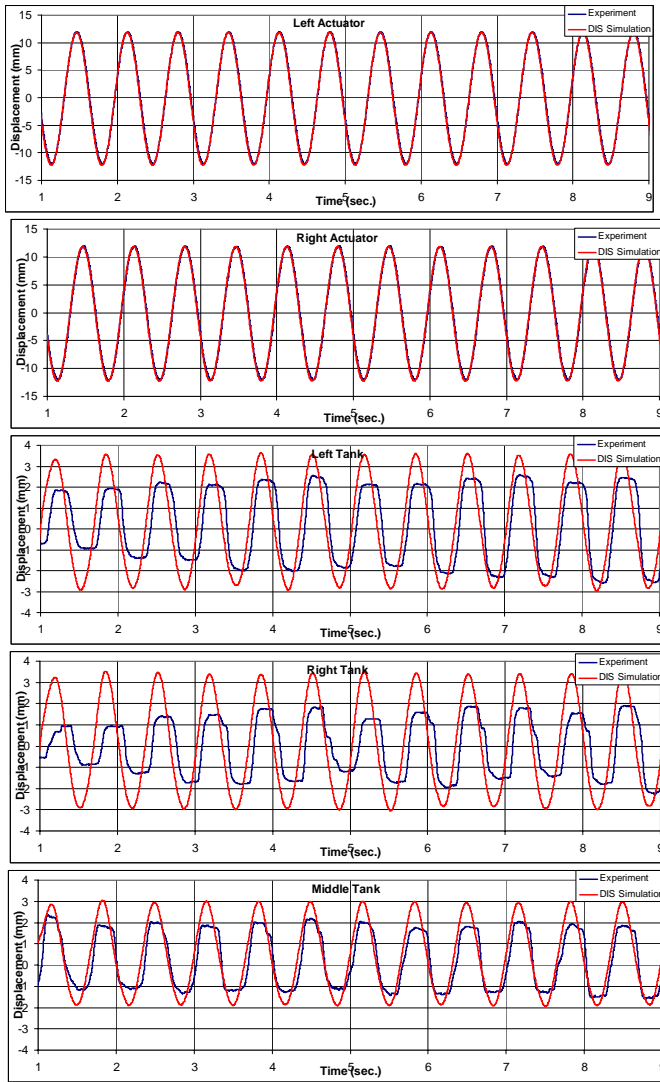
Figure 5 Comparison between experiment and DIS simulation for an empty tank with a pitch 3 Hz, 6 mm harmonic excitation. Top 2 graphs show the input motion of the actuator. Bottom three graphs show the resulting motion of the 3 suspension springs.
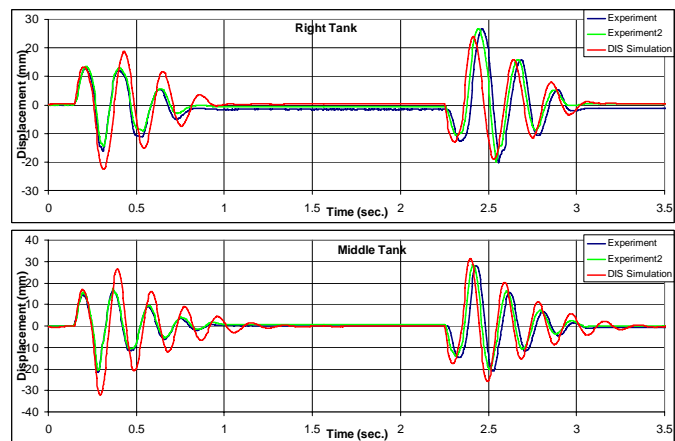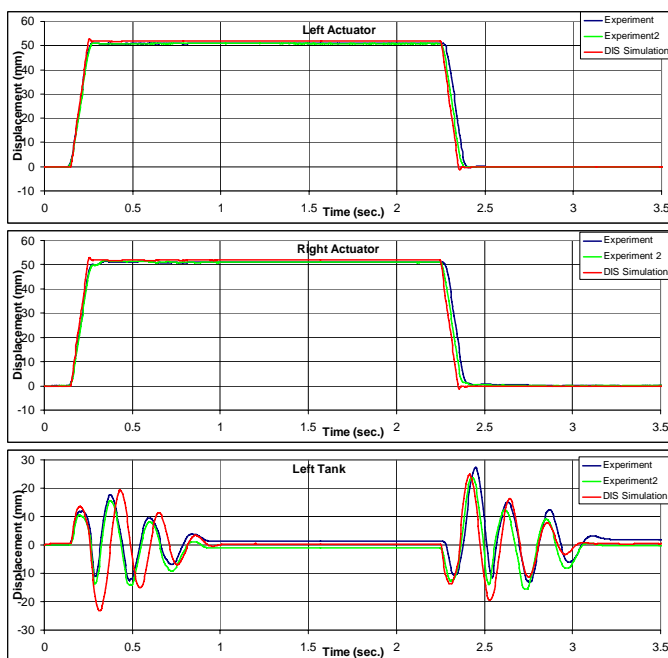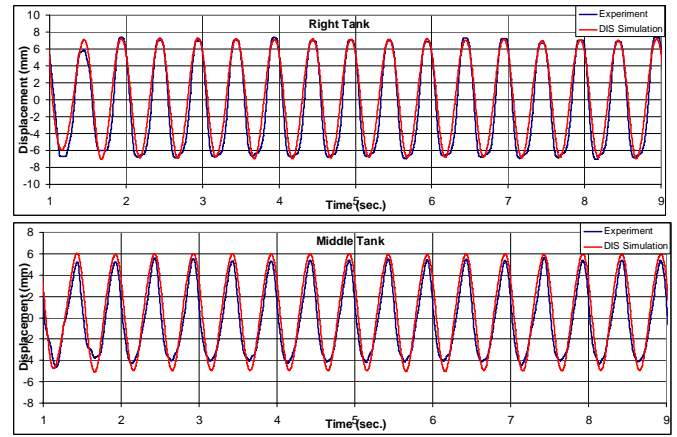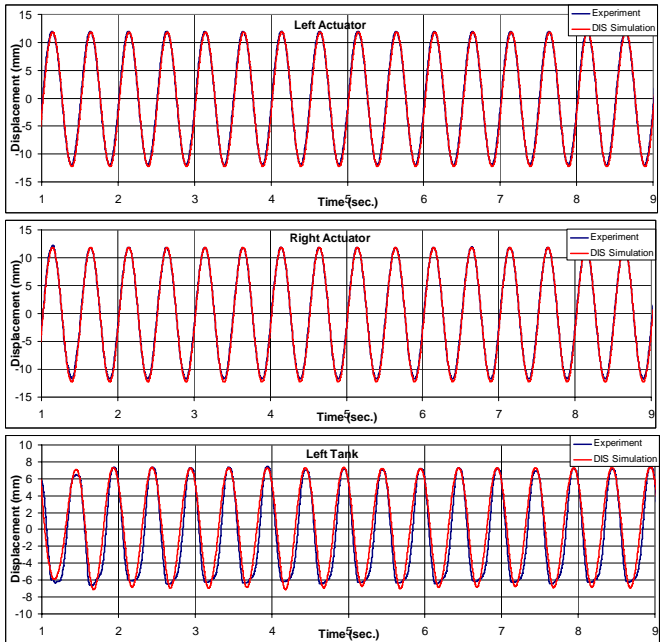

Figure 6 Comparison between experiment and DIS simulation for empty tank pitch 52 mm ramp excitation.
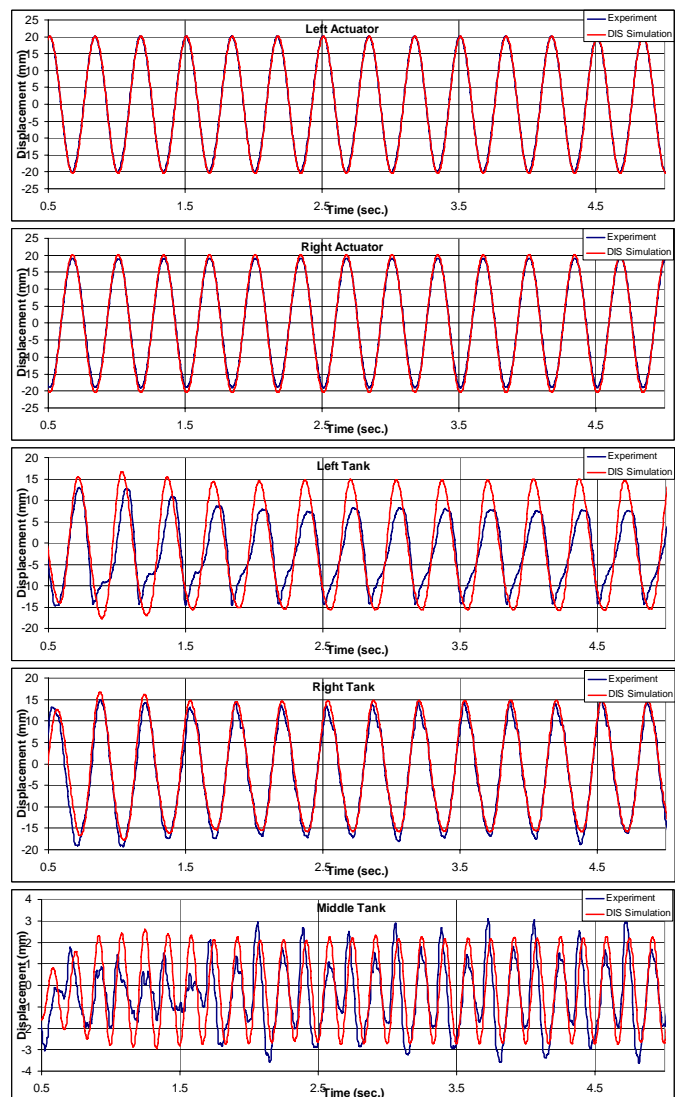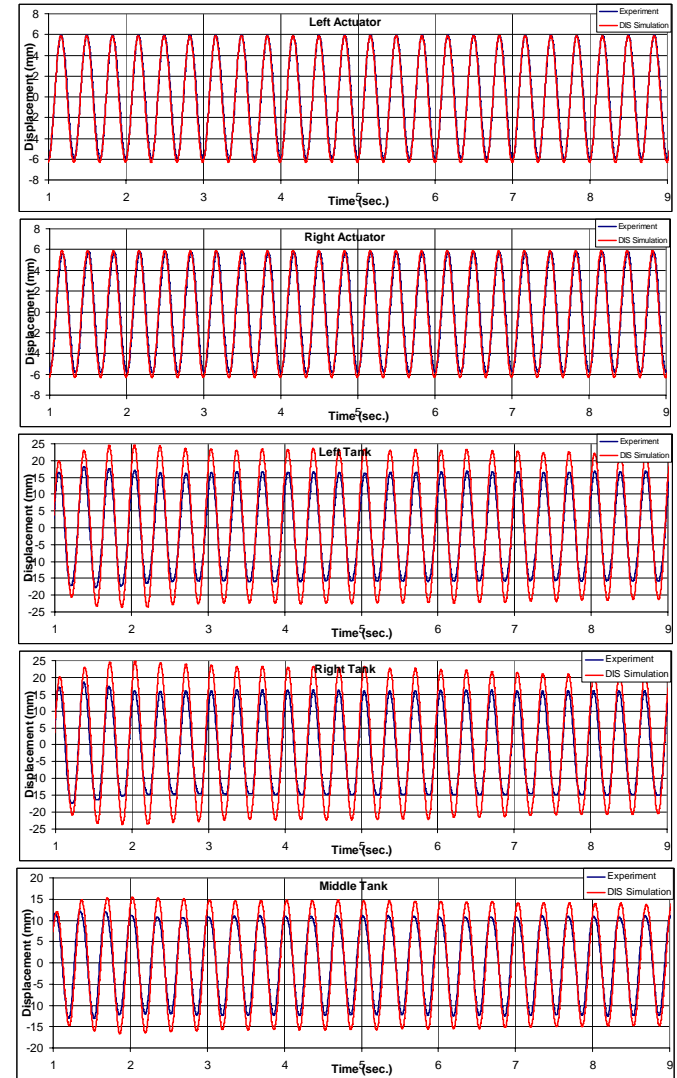

Figure 7 Comparison between experiment and DIS simulation for empty tank roll 3 Hz, 20 mm harmonic roll excitation.
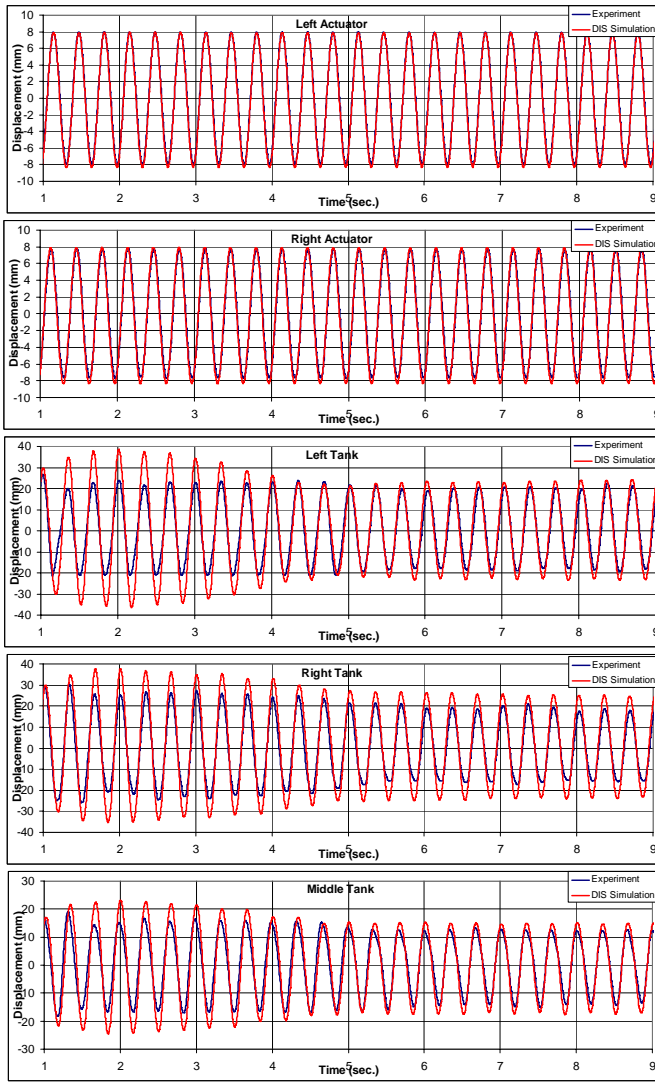
Figure 8 Comparison between experiment and DIS simulation for half-full tank with baffles pitch 1.5 Hz, 12 mm harmonic excitation.
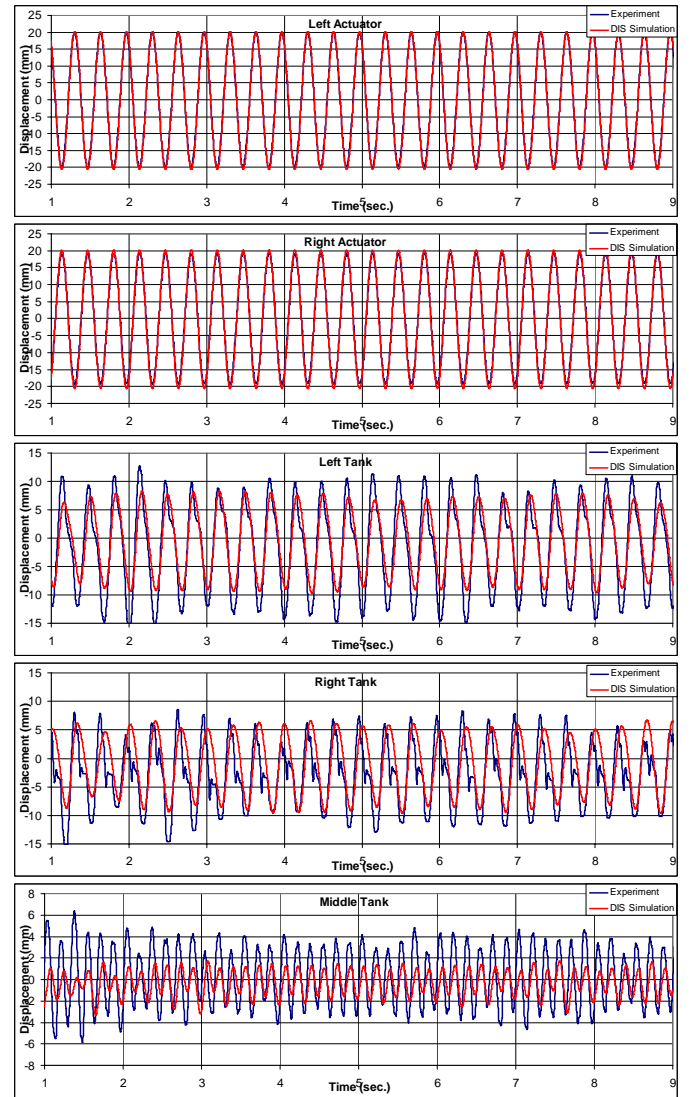

Figure 9 Comparison between experiment and DIS simulation for half-full tank with baffles pitch 2 Hz, 12 mm harmonic excitation.

Figure 10 Comparison between experiment and DIS simulation for half-full tank with baffles pitch 3 Hz, 6 mm harmonic excitation.
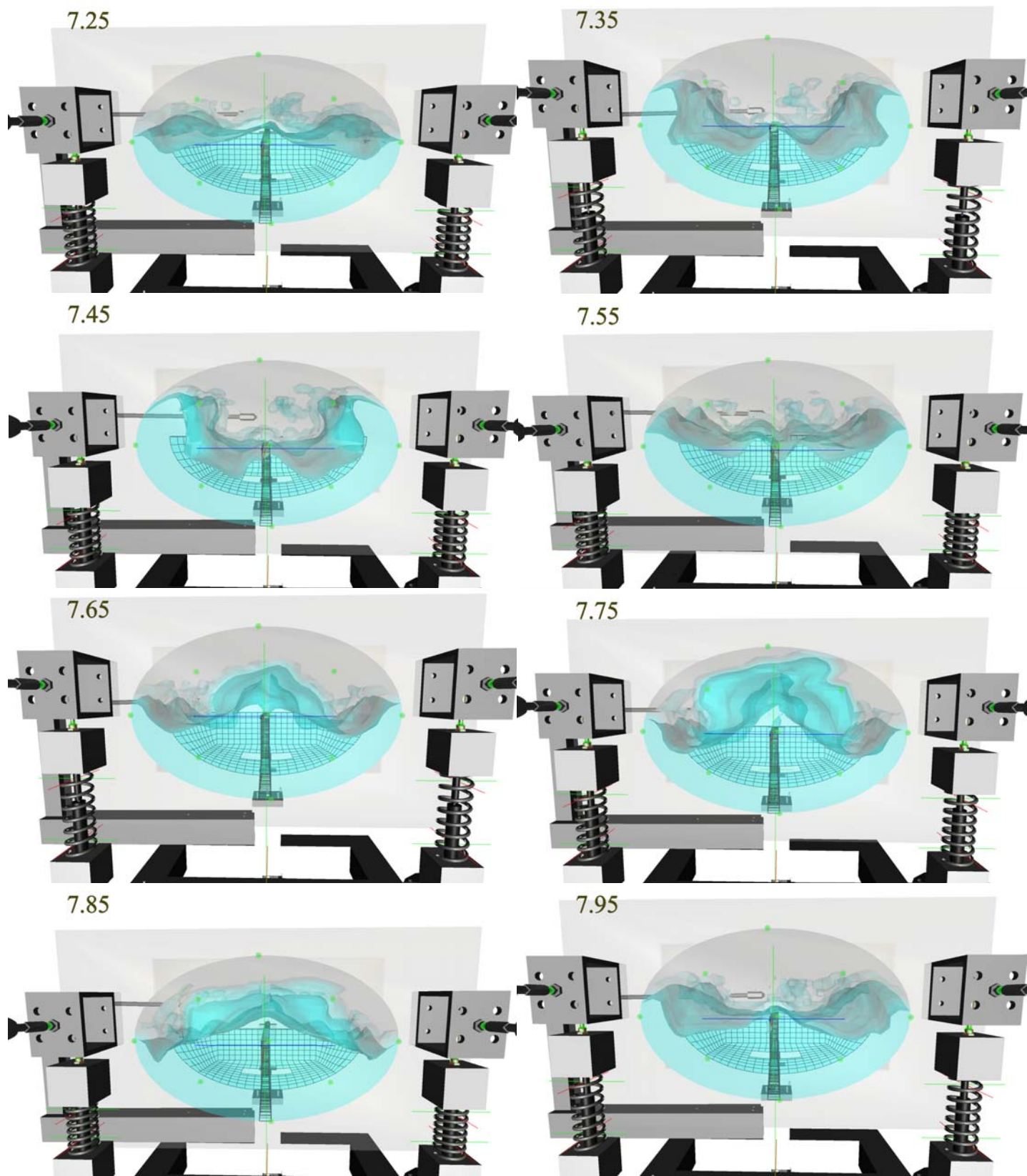
Figure 11 Comparison between experiment and DIS simulation for half-full tank with baffles pitch 3 Hz, 8 mm harmonic excitation.
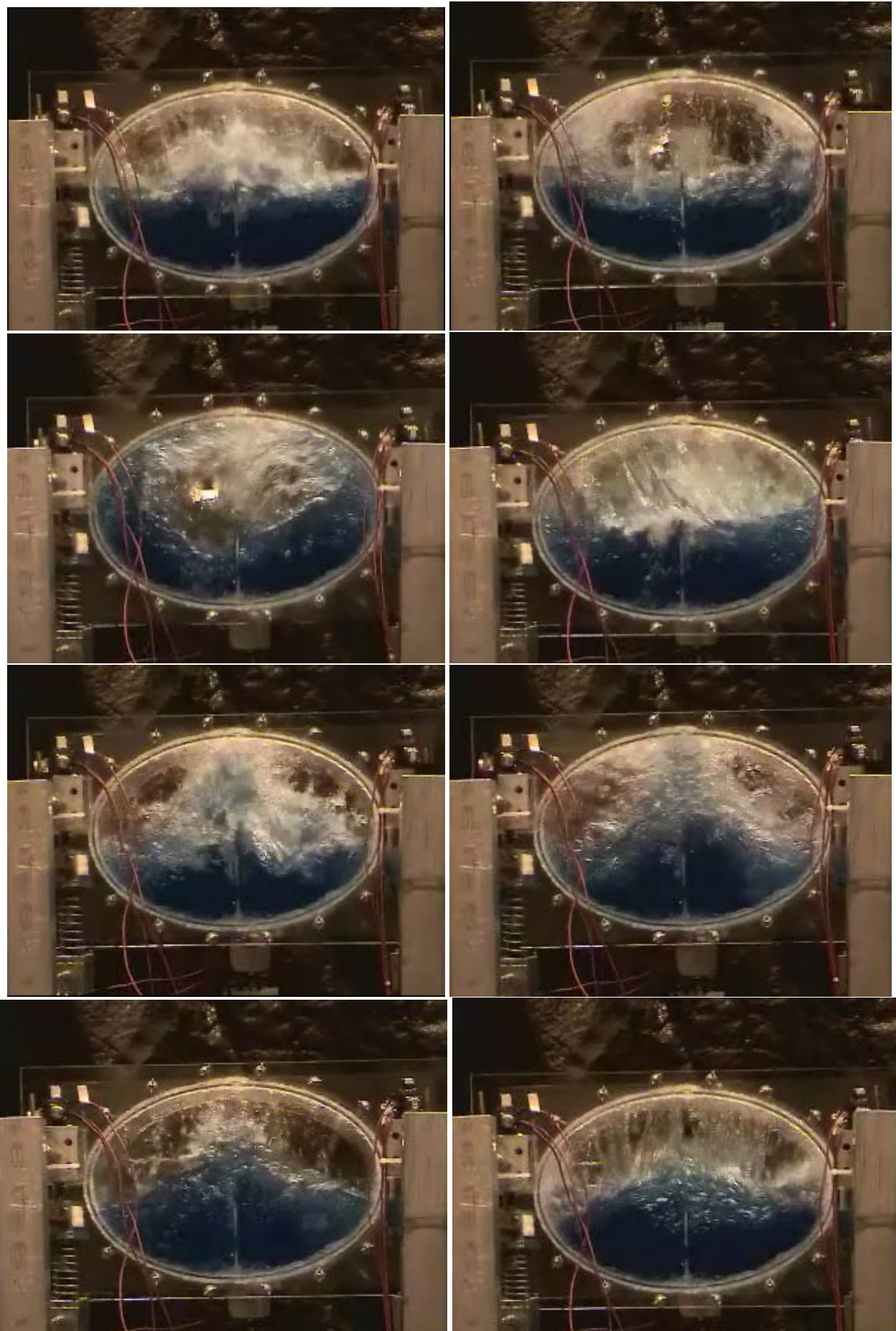

Figure 12 Comparison between experiment and DIS simulation for half-full tank with baffles roll 3 Hz, 20 mm harmonic excitation.
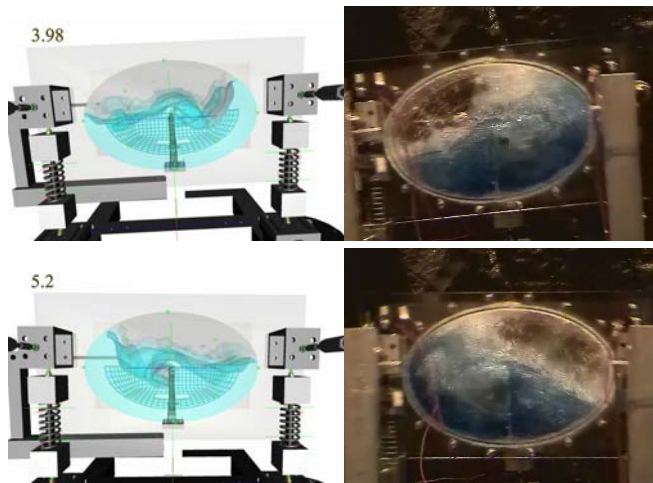
Figure 13 DIS simulation snapshots of the front view of the half-filled tank with baffles at 3 Hz, 8 mm pitch excitation.

Figure 14 Experiment snapshots of the front view of the half-filled tank with baffles at 3 Hz, 8 mm pitch excitation taken at approximately the same times as the snapshots in Figure 13.

Figure 15 Simulation and experiment snapshots for half-full tank with baffles roll 2 Hz, 30 mm harmonic excitation.

Table 3 shows the experiments carried out with an empty tank. Those experiments are used to characterize the suspension spring stiffness, damping and friction properties, as well as to validate the solid multibody dynamics solution. Twelve empty tank experiments are carried out. Figure 5 shows the comparison of the experiment and simulation results for a 3 Hz, 6 mm pitch harmonic excitation with an empty tank. Since both the right and left actuators are moving the same amount, then the left and right springs should also move the same amount. The experiment shows that the magnitude of motion of the left spring is about 10 mm while the magnitude of motion of the right spring is 8 mm. The DIS simulation predicts that the magnitude of motion of both springs is about 7 mm. The experiment response and simulation response of the middle-spring are practically coincident.

Figure 6 shows a comparison of the experiment and simulation results for a 52 mm pitch ramp excitation of the empty tank. Figure 7 shows a comparison of the experiment and simulation results for a 3 Hz, 20 mm harmonic roll excitation for the empty tank. Figures 5-7 show that the multibody dynamics model of the test fixture without fluid in the tank can predict with an average difference of about 15% the response of the actual test fixture. The difference between the results can be mostly attributed to:

• Non-linear behavior of the suspension struts, including non-linear damping/friction and clearances.

• Imprecision of the spherical joints of the test fixture. This includes joint clearances and friction.

This is evident from the fact that in Figure 5-7 the amplitude of motion of the right and left springs are different by about an average of 15%, while if the test fixture joints and suspension springs were ideal, the difference between the response of the left and right springs should be much smaller (~5% similar to the difference exhibited in the simulation).

Figures 8-11 show a comparison of the experiment and simulation results for various harmonic pitch excitations

of a half-full tank. In Figure 8 the excitation is 1.5 Hz and 12 mm. In Figure 9 it is 2 Hz, 12 mm. In Figure 10 it is 3 Hz, 6 mm and in Figure 11 it is 3 Hz, 8 mm. Figure 12 shows a comparison of the experiment and simulation results for a 3 Hz, 20 mm harmonic roll excitation for the half-full tank. Figures 8-12 show that the DIS simulation predicts the response of the test fixture with half-full tank within an average of difference of 15% from the experiments, which is the same average difference between model and experiment as with the empty tank runs. This suggests that the difference between the experiment and simulation is mostly due to the non-linear behavior of the test fixture suspension struts and spherical joints. Figures 7 and 10 show that for the roll excitation the liquid sloshing in the tank reduces the motion of the suspension springs. This is due to the fact that in roll motion, the fluid acts like a load balancer, thus limiting the transfer of forces from the tank to the springs.

Figure 13 shows snapshots of the front view of the half-filled tank with baffles at 3 Hz, 8 mm pitch excitation. Figure 14 shows snapshots taken from the front view experiment camera at approximately the same times as the snapshots in Figure 13. Figures 13 and 14 show that the shape and mode of motion of the liquid's free surface predicted by the model is approximately the same as the experiment. Figures 11, 13 and 14 show that at 3 Hz, 8 mm harmonic pitch excitation, the liquid sloshing undergoes a mode change from a straight up-down motion along with the tank to a symmetric sine sloshing motion along the tank cross-section. When the liquid undergoes this mode change, the amplitude of motion of the suspension springs is reduced by about 25%. Note both the simulation and experiment show that this mode change does not occur at 3 Hz, 6mm harmonic pitch excitation (Figure 10).

Figure 15 shows two snapshots of the front view of the half-filled tank with baffles at 2 Hz, 30 mm roll excitation.

8. CONCLUDING REMARKS

A finite element model for predicting the fully coupled dynamic response of flexible multibody systems and liquid sloshing in containers was presented. The model has the following characteristics:

• Parallel explicit time-integration solver.

• Library of accurate large rotation finite elements including: truss, beam, shell and solid elements. The elements only use Cartesian coordinates as DOFs.

• The fluid mesh is modeled using a very light and compliant solid mesh which allows the fluid mesh to move/deform along with the tank using the Arbitrary Lagrangian-Eulerian formulation.

• Acceptor-donor VOF algorithm for modeling the fluid's free-surface.

• The motion of the solid and fluid is referred to a global inertial Cartesian reference frame.

- A total Lagrangian deformation description is used for the solid elements.

- The penalty technique is used to model the joints.

A validation study of the finite element model was carried out using a specially designed test-fixture. The study shows that the model can predict reasonably well (within 15% on average) the response measured on the physical test fixture.

ACKNOWLEDGEMENTS

REFERENCES

1. Gerrits, J. and Veldman, A., "Numerical simulation of coupled liquid-solid dynamics," *European Congress on Computation Methods in Applied Science and Engineering*, ECCOMAS 200, Barcelona, 2000.
2. Fekken, G., "Numerical simulation of a free-surface flow with moving rigid bodies," *Ph.D. Dissertation,* University of Groningen, 2004.
3. Rumold, W., "Modeling and simulation of vehicles carrying liquid cargo", *Multibody System Dynamics,* Vol 5, pp. 351-374, 2001.
4. Tezduyar, T.E., "Finite element methods for flow problems with moving boundaries and interfaces," *Archives of Computational Methods in Engineering,* Vol. 8(2), pp. 8-130, 2001.
5. Walhorn, E., Kolke, A., Hubner, B., and Dinkler, D., "Fluid–structure coupling within a monolithic model involving free surface flows," *Computers and Structures*, Vol. 83, pp. 2100-2111, 2005.
6. Nomura, T., "ALE finite element computations of fluid-structure interaction problems," *Computer Methods in Applied Mechanics and Engineering,* Vol. 112(1-4), pp. 291-308, 1994.
7. Idelsohn, S.R., Onate, E, Del Pin, F. and Calvo, N., "Fluid-structure interaction using the particle finite element method," *Computer Methods in Applied Mechanics and Engineering*, Vol. 195(17-18), pp. 2100-2123, March 2006.
8. Hirt, C.R. and Nichols, B.D., "Volume of fluid (VOF) method for the dynamics of free boundaries," *Journal of Computational Physics*, Vol. 39, pp. 201-225, 1981.
9. Youngs, D.L., "An interface tracking method for a 3D Eulerian hydrodynamics code," *Technical Report AWRE/44/92/35,* Atomic Weapons Research Establishment, 1987.
10. Souli, M. and Zolesio, J.P., "Arbitrary Lagrangian-Eulerian and free surface methods in fluid mechanics," *Computer Methods in Applied Mechanics and Engineering,* Vol. 191, pp. 451-466, 2001.
11. Braess, H. and Wriggers, P., "Arbitrary Lagrangian Eulerian finite element analysis of free surface flows," *Computer Methods in Applied Mechanics and Engineering*, Vol. 190, pp. 95-109, 2000.
12. Stein, K. and Tezduyar, T., "Advanced mesh update techniques for problems involving large displacements," *Fifth world congress on computation* mechanics, WCCM V, Vienna, Austria, 2002.
13. *Bilarbegian, M. and Zu, J.W., "Dynamic analysis and simulation of vehicles carrying liquids during braking," ASME DETC2005-85102, 5th International Conference on Multibody Systems, Nonlinear Dynamics, and Control, ASME DETC, Long Beach, CA, 2005.*
14. *Wasfy, T.M. and Noor, A.K., "Computational Strategies for Flexible Multibody Systems," Applied Mechanics Reviews, 56(6), 553-613, 2003.*
15. *Wasfy, T.M. and Noor, A.K., "Modeling and sensitivity analysis of multibody syste`ms using new solid, shell and beam elements," Computer Methods in Applied Mechanics and Engineering, Vol. 138(1-4) (25th Anniversary Issue), pp. 187-211, 1996.*
16. *Wasfy, T.M., "A torsional spring-like beam element for the dynamic analysis of flexible multibody systems," International Journal for Numerical Methods in Engineering, Vol. 39(7), pp. 1079-1096, 1996.*
17. *Wasfy, T.M., "Edge projected planar rectangular element for modeling flexible multibody systems," 19th Biennial Conference on Mechanical Vibration and Noise, Paper No. DETC2003-48351, 19th Biennial Conference on Mechanical Vibration and Noise, ASME International 2003 DETC, Chicago, IL, 2003.*
18. *Wasfy, T.M., "Lumped-parameters brick element for modeling shell flexible multibody systems," 18th Biennial Conference on Mechanical Vibration and Noise, ASME International 2001 DETC, Pittsburgh, PA, 2001.*
19. *Wasfy, T.M., "Modeling spatial rigid multibody systems using an explicit-time integration finite element solver and a penalty formulation," ASME Paper No. DETC2004-57352, 28th Biennial Mechanisms and Robotics Conference, DETC, Salt Lake, Utah 2004.*
20. *Leamy, M.J. and Wasfy, T.M., "Transient and steady-state dynamic finite element modeling of belt-drives," ASME Journal of Dynamics Systems, Measurement, and Control, Vol. 124(4), pp. 575-581, 2002.*
21. *Wasfy, T.M. and Leamy, M.J., "Modeling the dynamic frictional contact of tires using an explicit finite element code," ASME DETC2005-84694, 5th International Conference on Multibody Systems, Nonlinear Dynamics, and Control, ASME DETC, Long Beach, CA, 2005.*
22. *Wasfy, T.M., "Asperity spring friction model with application to belt-drives," Paper No. DETC2003-48343, Proceeding of the DETC: 19th Biennial Conference on Mechanical Vibration and Noise, Chicago, IL, 2003.*

23. *Wasfy, T.M. and Leamy, M.J., "Dynamic modeling of synchronous belt-drives using an explicit finite element code," ASME DETC2005-85103, 5th International Conference on Multibody Systems, Nonlinear Dynamics, and Control, ASME DETC, Long Beach, CA, 2005.*

24. *Meckstroth, R.J., Wasfy, T.M., and Leamy, M.J., "Finite element study of the dynamic response of serpentine belt-drives with isolator clutches," SAE 2004 Congress, Paper No. 2004-01-1347, Detroit, MI, 2004.*

25. *Chorin, A.J., "A Numerical Method for Solving Incompressible Viscous Flow Problems," Journal of Computational Physics, Vol. 2(1), 1967.*

26. *Wasfy, T.M., West, A.C. and Modi, V., "Parallel finite element computations of unsteady incompressible flows," International Journal for Numerical Methods in Fluids, Vol. 26(1), pp. 17-37, 1998.*

27. *DIS (Dynamic Interactions Simulator), http://www.ascience.com/ScProducts.htm, Advanced Science and Automation Corp., 2006.*